

# Structural Changes of Cytochrome $c_{552}$ from *Thermus thermophilus* Adsorbed on Anionic and Hydrophobic Surfaces Probed by FTIR and 2D-FTIR Spectroscopy

Sophie Lecomte,<sup>\*,[a]</sup> Christophe Hilleriteau,<sup>[a]</sup> Jean Pierre Forgerit,<sup>[a]</sup> Madeleine Revault,<sup>[a]</sup> Marie-Hélène Baron,<sup>[a]</sup> Peter Hildebrandt,<sup>[b]</sup> and Tewfik Soulimane<sup>[c]</sup>

The structural changes of cytochrome  $c_{552}$  bound to anionic and hydrophobic clay surfaces have been investigated by Fourier transform infrared spectroscopy. Binding to the anionic surface of montmorillonite is controlled by electrostatic interactions since addition of electrolyte ( $0.5 \text{ mol L}^{-1} \text{ KCl}$ ) causes desorption of more than  $2/3$  of the protein molecules. Electrostatic binding occurs through the back side of the protein (i.e., remote from the heme site) and is associated only with subtle changes of the secondary structure. In contrast, adsorption to the hydrophobic surface of talc leads to a decrease in  $\alpha$ -helical structure by ca. 5% and an increase in  $\beta$ -sheet structure by ca. 6%. These structural changes are attributed to a hydrophobic region on the front surface of cytochrome  $c_{552}$  close to the partially exposed heme edge. This part on the protein surface is identified as the interaction domain for talc and most likely also serves for binding to the natural reaction partner, a  $\text{ba}_3$ -oxidase. Fourier transform infrared spectra of cytochrome  $c_{552}$  and the clay–cytochrome  $c_{552}$  complexes have been measured as a function of time following dissolution and

suspension in deuterated buffer, respectively. A two-dimensional correlation analysis was applied to these spectra to investigate the dynamics of the structural changes in the protein. For both complexes, adsorption and subsequent unfolding processes in the binding domains are faster than the time resolution of the spectroscopic experiments. Thus, the processes that could be monitored are refolding of peptide segments and side chain rearrangements following the adsorption-induced perturbation of the protein structure and the solvation of the adsorbed protein. In each case, side chain alterations of solvent-exposed tyrosine, aspartate, and glutamate residues were observed. For the cytochrome  $c_{552}$ –talc complex, these changes are followed by a slow refolding of the peptide chain in the binding domain and, subsequently, a further H/D exchange of amide group protons.

## KEYWORDS:

cytochromes · electron transport · heme proteins · IR spectroscopy · protein structures

## Introduction

In the respiratory chain of aerobic organisms, cytochrome  $c$  (Cyt- $c$ ) acts as a mediator for the electron transport between complexes III (cytochrome  $c$  reductase) and IV (cytochrome  $c$  oxidase, CcO).<sup>[1, 2]</sup> Binding of Cyt- $c$  to its reaction partners is governed by electrostatic interactions involving various positively charged lysine residues on the front hemisphere of Cyt- $c$ . Among these lysines, Lys-73 and Lys-79 have been shown to play a crucial role for inducing conformational changes in Cyt- $c$  upon complex formation with CcO.<sup>[3]</sup> These structural changes are associated with a substantial lowering of the redox potential corresponding to an increase in the driving force for the interprotein electron transfer process to CcO.<sup>[3, 4]</sup> Hence, the lysine-rich domain around the exposed heme edge may be of functional relevance for regulating the biological redox process.


Such a cationic domain was regarded as a common structural template for soluble type- $c$  cytochromes until it was recently shown that cytochrome  $c_{552}$  (Cyt- $c_{552}$ ), which serves as an

electron carrier in the respiratory chain of *Thermus thermophilus*,<sup>[5, 6]</sup> does not exhibit a cluster of lysine residues on the protein surface<sup>[7]</sup> (space-filling plots of the structure of Cyt- $c_{552}$ , given in the Supporting Information, show the localization of the hydro-

[a] Dr. S. Lecomte, C. Hilleriteau, J. P. Forgerit, M. Revault, Dr. M.-H. Baron  
Laboratoire de Dynamique, Interactions et Réactivité  
UMR-7075, CNRS-Université Paris VI  
2 rue Henri Dunant, 94320 Thiais (France)  
Fax: (+33) 1-49-78-11-18  
E-mail: Sophie.Lecomte@glvt-cnrs.fr

[b] Prof. Dr. P. Hildebrandt  
Max-Planck-Institut für Strahlenchemie  
Stiftstrasse 34–36, 45470 Mülheim (Germany)

[c] Dr. T. Soulimane  
Institut für Biochemie, Klinikum Aachen  
Pauwelsstrasse 30, 52057 Aachen (Germany)

 Supporting information for this article is available on the WWW under <http://www.chembiochem.com> or from the author.

phobic and cationic residues on the surface of the protein). Cyt-*c*<sub>552</sub> possesses also a more stable structure compared to Cyt-*c*, brought about by ca. 1/3 of the C-terminal peptide chain that wraps around the remainder of the protein.<sup>[7]</sup> This largely uncharged peptide segment partly shields the heme pocket on the front surface of the protein. This unique structural property of Cyt-*c*<sub>552</sub>, therefore, raises fundamental questions with respect to the molecular mechanism of the electron transfer process to the membrane-bound reaction partner, a *ba*<sub>3</sub>-oxidase; particularly since in contrast to CcO, the putative binding site of *ba*<sub>3</sub>-oxidase lacks any negatively charged residues as revealed by the X-ray crystal structure.<sup>[8]</sup> Specifically, it has to be determined if a conformational control of the biological electron transfer as suggested for the Cyt-*c*/CcO redox couple<sup>[9]</sup> may be also of relevance for the reaction of Cyt-*c*<sub>552</sub> with the *ba*<sub>3</sub>-oxidase.<sup>[9]</sup> As a prerequisite for a comparative analysis of the interprotein electron transfer mechanisms, a detailed knowledge about the intermolecular interactions between Cyt-*c*<sub>552</sub> and the *ba*<sub>3</sub>-oxidase and the possible structural consequences is required.

In the present work, we have addressed this issue by studying the effect of different modes of intermolecular interactions on the structure of Cyt-*c*<sub>552</sub>. Model systems were used that exhibit either anionic or uncharged surfaces and, hence, may bind Cyt-*c*<sub>552</sub> through electrostatic or hydrophobic forces, respectively. Montmorillonite (MT) and talc (TC) clays were chosen as models for anionic and hydrophobic binding domains, respectively. Both clays offer the advantage of a high specific surface area providing a large amount of bound Cyt-*c*<sub>552</sub> per volume. Furthermore, these model systems are largely "silent" with respect to those spectroscopic techniques that are capable of probing the structure of the adsorbed protein.

In this study, we have employed Fourier transform infrared (FTIR) spectroscopy, which has been shown to be sensitive for detecting subtle adsorption-induced modifications of the secondary and tertiary structure of protein as well as hydration changes of the polypeptide backbone and amino acid side chains.<sup>[10]</sup> Furthermore, FTIR spectra recorded as a function of time, have been analyzed in a two-dimensional (2D) way,<sup>[11]</sup> providing information about the time dependence of the structural modifications of individual protein segments. These investigations give insight into the dynamics specifically of those parts of Cyt-*c*<sub>552</sub> that are involved in binding to the model surfaces. Thus, the results may contribute to a better understanding of the Cyt-*c*<sub>552</sub>–*ba*<sub>3</sub>-oxidase interactions at the molecular level and may elucidate similarities and differences with respect to the mitochondrial redox couple Cyt-*c*/CcO.

## Experimental Section

**Materials:** Cyt-*c*<sub>552</sub> from *T. thermophilus* was isolated and purified as described previously.<sup>[5]</sup> Lyophilization of the protein is required for the FTIR experiments. The Wyoming-type MT [(Al<sub>1.32</sub>Fe<sub>0.06</sub>Mg<sub>0.71</sub>)(Si<sub>3.95</sub>Al<sub>0.5</sub>)O<sub>10</sub>(OH)<sub>2</sub>] used in the experiments exhibits a particle size < 2 μm, a specific surface of 800 m<sup>2</sup>g<sup>-1</sup>, and a surface charge of 1.25 × 10<sup>-6</sup> C m<sup>-2</sup>.<sup>[12]</sup> TC [Mg(Si<sub>8</sub>O<sub>20</sub>)(OH)<sub>4</sub>] (Luzenac) was of a similar

size (< 2 μm) with a specific surface area of 18.5 m<sup>2</sup>g<sup>-1</sup>.<sup>[13]</sup> Deuterated buffer solutions were prepared with K<sub>2</sub>DPO<sub>4</sub> (0.05 mol L<sup>-1</sup>) obtained upon repeated crystallization of K<sub>2</sub>HPO<sub>4</sub> in D<sub>2</sub>O. In all samples, the pH value was adjusted to 8.0 by addition of DCl.

**Sample preparation:** Solutions of Cyt-*c*<sub>552</sub> were obtained by dissolving the lyophilized protein in deuterated buffer to a final concentration of 4 mg mL<sup>-1</sup>. Complexes of Cyt-*c*<sub>552</sub> with MT and TC were prepared by suspending a mixture of solid protein and clay in the buffer with final MT and TC concentrations of 8 and 200 mg mL<sup>-1</sup>, respectively. The different MT and TC concentrations were chosen to compensate for the large difference in specific area of the two clays. The concentration of Cyt-*c*<sub>552</sub> was 4 mg mL<sup>-1</sup> in each case. Samples of high ionic strength were obtained by addition of KCl (0.5 mol L<sup>-1</sup>). FTIR spectra were obtained from the Cyt-*c*<sub>552</sub>–clay suspensions as well as from the solid samples or supernatants obtained after centrifugation of the suspensions. This procedure also allowed to determine the amount of protein adsorbed on the clays.

**FTIR spectroscopic measurements:** FTIR transmission spectra were recorded with a Perkin Elmer 1720 interferometer (four scans; 4 cm<sup>-1</sup> resolution). A Balston air dryer (Whatman) was used to reduce the water vapor content in the spectrometer. Protein–clay suspensions were deposited between two CaF<sub>2</sub> plates with a 25-μm spacer whereas Cyt-*c*<sub>552</sub> solutions were measured by using a CaF<sub>2</sub> cell with a 50-μm spacer. The FTIR spectra were recorded in the time range from 10 min to 5 h subsequent to the preparation of the sample. The addition of buffer to the dry protein and protein–clay mixture was taken as the starting point of the processes under investigation. The FTIR spectra measured after five hours were taken as the reference for equilibrium conditions.

**Analysis of the FTIR spectra:** Prior to the analysis of spectra, the spectral contributions of the buffer and of the adsorbents were subtracted from the measured spectra. These difference spectra were analyzed by algorithms based on second-derivative functions<sup>[14]</sup> and self-deconvolution procedures in order to determine the number and the frequencies of individual band components contained in the spectral range 1500–1750 cm<sup>-1</sup> (Figure 1). The relative contributions of the various band components were obtained by a band-fitting procedure, keeping the wavenumbers, half widths (14–20 cm<sup>-1</sup>) and band profiles (75% Gaussian and 25% Lorentzian) constant and allowing only the intensities to vary. All spectra could be fitted by seven amide-I and two amide-II components along with a few bands assigned to amino acid side chains. The content of the various secondary structure elements was estimated by dividing the integral intensity of one amide-I band component by the total intensity of all amide-I band components. The amount of each secondary structure element is given in percentage terms. In the same way, the integral amide-II band intensities are normalized. Taking into account the number of peptide bonds of Cyt-*c*<sub>552</sub>,<sup>[7]</sup> an intensity redistribution among the amide-I bands can be quantified in terms of secondary structure changes, that is, an intensity change of the amide-I bands by 2% is related to 2–3 peptide bonds. The amide-II/amide-I band intensity ratio is used to assess the degree of H/D exchange using a reference value of 0.5 for totally hydrogenated proteins in the solid state, according to a study of various globular proteins in the solid state.<sup>[15]</sup> Thus, a decrease of this ratio by 2% corresponds to the exchange at 4–6 amide NH groups. These estimations neglect contributions of Asn and Gln amide side chains to the amide-I band envelope. As is shown below, this approximation results in a constant and systematic error of the *absolute* secondary structure determination whereas the effect on determining *changes* of the secondary structure and of the degree of H/D exchange are negligibly small.

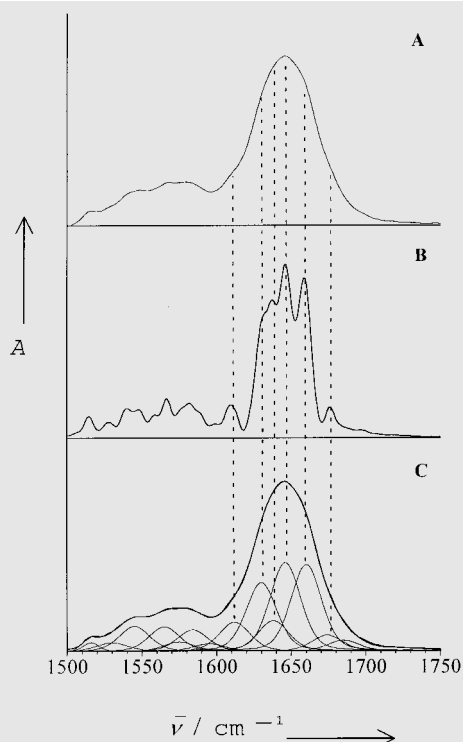


**Figure 1.** FTIR spectra of Cyt- $c_{552}$  in deuterated buffer (pD 8.0). A: Experimental spectrum obtained after subtracting the buffer contribution. B: Spectrum showing individual band components obtained from second-derivative analysis. C: Experimental spectrum including the band components. See text for details.

**2D-FTIR analysis:** The 2D analysis of the FTIR spectra followed the procedure introduced by Noda.<sup>[11]</sup> It allows the correlation of the dynamic fluctuations of IR signals in a series of spectra measured at different times. Cross correlation analysis provides 2D spectra that are defined by two independent wavenumbers,  $\tilde{\nu}_1$  (abscissa) and  $\tilde{\nu}_2$  (ordinate). The synchronous correlation representation (S-map) displays autopeaks on the diagonal reflecting those IR signals that vary as a function of time. Cross peaks (placed off-diagonally) are observed for bands that exhibit (at least partially) correlated dynamic behavior. Cross peaks, which can either be positive or negative, reflect correlated changes of functional groups within the protein that occur simultaneously in the same (+) or in the opposite direction (-). Conversely, the asynchronous 2D correlation representation (A-map) is characterized by missing autopeaks and asymmetric cross peaks which reveal noncorrelated (i.e., out-of-phase) behavior of two bands. Positive cross peaks refer to IR signals that vary in the same direction, that is, intensity increase or decrease. Intensity changes of peaks in opposite directions give rise to negative cross peaks. Peaks that exhibit no intensity changes in the series of spectra do not appear in the 2D maps.

Cross peaks, which occur in both the S- and the A-maps, provide information about the temporal order of the spectral changes. Cross peaks with the same sign in the S- and A-maps indicate that a spectral change of the IR signal with wavenumbers  $\tilde{\nu}_2$  (ordinate) precedes that of the  $\tilde{\nu}_1$  signal (abscissa). For opposite signs of the S- and A-map cross peaks, the temporal order is reversed. In our 2D-FTIR analysis, we will discuss only cross peaks observed in both the S- and the A-maps since this is a prerequisite to determining the order of the different events.

In the present study, the time-dependent changes of the IR signals reflect the structural and solvation changes of Cyt- $c_{552}$  brought about

by dissolution in buffer and/or adsorption on clay. In general, six spectra were considered that cover the time range from 10 min to 5 h. The auto- and cross peaks in the S- and A-maps were found at frequencies very similar to those of the band components determined by deconvolution and band fitting of the FTIR spectra, indicating that the 2D and the conventional spectra analysis afford consistent results.

## Results and Discussion

### Assignments

The spectral region between 1600–1700  $\text{cm}^{-1}$  is dominated by the amide-I mode of the polypeptide backbone of Cyt- $c_{552}$ . There is a large body of experimental data that allows an assignment of the individual amide-I band components to various secondary structure elements of proteins (Table 1).<sup>[10, 15, 16]</sup> Upon H/D exchange this mode, which predominantly includes the C=O stretching of the peptide bond, reveals only a subtle frequency

**Table 1.** Vibrational assignments of the IR bands of Cyt- $c_{552}$ .

Mode	$\tilde{\nu}$ [ $\text{cm}^{-1}$ ] <sup>[a]</sup>		Description
	FTIR	2D-FTIR	
<i>backbone</i>			
amide I	1697		<i>secondary structure element</i> $\beta$ -strands in apolar domains
	1676	1678	not hydrogen-bonded inside the protein core
	1660	1656	hydrogen-bonded in irregular/internal $\alpha$ -helix
	1646	1646	hydrogen-bonded in regular/external $\alpha$ -helix
	1638		hydrated in random-coil domains
	1630	1625	hydrogen-bonded in $\beta$ -strands or turns
amide II	1612	1616	hydrogen-bonded in protein self-association
	1546	1546	strongly hydrogen-bonded NH
	1530	1530	weakly hydrogen-bonded NH
<i>side chains</i>			
$\nu(\text{C}=\text{C})$	1612	1612	Tyr
		1605	
$\nu(\text{C}=\text{C})$	1595	1595	Trp, His
	1584	1584	carboxylate (Asp)
$\nu_{\text{a}}(\text{COO}^-)$	1575	1575	carboxylate (Glu, Asp)
	1565	1565	carboxylate (Glu)
$\nu(\text{C}=\text{C})$	1516	1512	Tyr

[a] Frequencies refer to bands determined by second-derivative analysis (FTIR) or to auto- or cross correlation peaks observed in the 2D S-maps.

shift. Furthermore, H/D exchange was generally fast on the time scale of the FTIR experiments (i.e., < 10 min) and led to comparable high degrees of amide N–H deuteration between 80 and 90% for each sample. Thus, it appeared to be justified not to distinguish between the amide-I (nondeuterated) and amide-I' bands (deuterated) since the underlying error in the analysis of the FTIR spectra is small and systematic.<sup>[10]</sup>

The amide-I region also includes the C=O stretching modes of the side chains of three Asn and ten Gln residues, all of them being solvent-exposed. Thus, these modes should give rise to bands at 1650 and 1635  $\text{cm}^{-1}$  for the Asn and Gln residues, respectively,<sup>[17, 18]</sup> with molar extinction coefficients comparable to those for an amide-I band of the polypeptide backbone.<sup>[17b]</sup> These bands were not considered in the band-fitting analysis, leading to an overestimation of the relative contributions of the

amide-I band components that are specifically indicative of peptide bonds in random-coil domains (1638 cm<sup>-1</sup>) and  $\beta$  strands or turns (1630 cm<sup>-1</sup>), and, to a minor extent, of  $\alpha$ -helical structures (1660 and 1646 cm<sup>-1</sup>). Furthermore, for both the dissolved and the adsorbed Cyt-*c*<sub>552</sub>, the 2D analysis of the FTIR spectra revealed no indication for time-dependent changes of Asn/Gln side chains implying that such changes, if they occur at all, are fast compared to the time resolution of the experiments. Consequently, the contribution of the Asn/Gln side chains to the amide-I band is constant in all spectra measured of a given sample, that is, the error of the secondary structure determination is constant and systematic so that time-dependent spectral changes in the amide-I band region truly reflect secondary structure changes.

The cross peak observed at 1605 cm<sup>-1</sup> in the 2D-FTIR maps is assigned to an aromatic ring mode of Tyr residues (see below). This band was not explicitly taken into account in the band fitting and deconvolution of the FTIR spectra so that it contributes to the 1612-cm<sup>-1</sup> band component of the amide-I envelope (Table 1). This also led to an overestimation of the number of peptide bonds involved in protein self-association.

The amide-II mode involves the N-H in-plane bending coordinate and disappears upon H/D exchange so that the total intensity of the amide-II bands is an appropriate marker for monitoring the H/D exchange. This mode is assigned to bands at 1530 and 1546 cm<sup>-1</sup> corresponding to weakly and strongly hydrogen-bonded amide groups, respectively.<sup>[19]</sup> Note that the 2D S-map of Cyt-*c*<sub>552</sub> in solution also reveals a correlation peak at 1555 cm<sup>-1</sup> which is assigned to an amide-II mode (see above).

The asymmetric carboxylate stretching mode of the three Asp and nine Glu residues gives rise to the bands at 1584 and 1565 cm<sup>-1</sup>, respectively (Table 1).<sup>[17, 18]</sup> All Asp and Glu residues are ionized at pH 7.6 due to their solvent-exposed positions on the protein surface. Moreover, no band was detected in the 1700–1780-cm<sup>-1</sup> range assigned to the COOH functions. The band at 1575 cm<sup>-1</sup> is assigned to carboxylate groups of either Glu or Asp residues in different environments,<sup>[17c]</sup> whereas the band at 1595 cm<sup>-1</sup> is ascribed to the aromatic side chains of the single Trp and/or the three His residues.

### Solvation effects on the Cyt-*c*<sub>552</sub> structure

The analysis of the amide-I region in the FTIR spectrum of Cyt-*c*<sub>552</sub> dissolved in deuterated buffer yields the relative contributions of the various secondary structure elements. The data that are listed in Table 2 refer to the spectra measured 5 h after dissolution of the protein. Taking into account the number of Asn (3) and Gln residues (10) and the total number of peptide bonds (130), the neglect of these side chain contributions in the analysis of the amide-I band region (see above) causes an overestimation of the  $\beta$ -strands/turns and random coils of less than 3 and 2% (absolute percentage), respectively. For the total  $\alpha$ -helix content this error is even smaller and, in fact, the value obtained from the FTIR analysis (49%) agrees very well with the data derived from the crystal structure (48%).<sup>[7]</sup>

**Table 2.** Secondary structure elements of Cyt-*c*<sub>552</sub> dissolved in deuterated buffer.<sup>[a]</sup>

Secondary structure element	Relative contribution [%] <sup>[b]</sup>		
	sample 1	sample 2	sample 1 + KCl
$\beta$ -strands in apolar domains	1.5	1.5	1.6
not hydrogen-bonded inside the protein core	9	9.2	8.9
hydrogen-bonded in irregular/internal $\alpha$ -helix	26.5	25.8	26.1
hydrogen-bonded in external/regular $\alpha$ -helix	22.9	22.7	24.3
hydrated in random-coil domains	10.8	10.5	10
hydrogen-bonded in $\beta$ -strands or turns	20.8	21.7	21
hydrogen-bonded in protein self-association	8.5	8.6	8.1

[a] Determined from the FTIR spectrum measured after 5 h. [b] The results were obtained from two different samples (1, 2) at low ionic strength and from sample 1 after addition of KCl (0.5 mol L<sup>-1</sup>). The accuracy of the secondary structure determination is discussed in the text.

The average absolute deviation for the results obtained for two different Cyt-*c*<sub>552</sub> samples (1, 2) measured under the same conditions is ca. 1.5%, which obviously reflects the reproducibility of the experiments and the band-fitting accuracy since similar deviations were found for the adsorbed Cyt-*c*<sub>552</sub>. Thus, we consider intensity variations of amide-I band components of more than 2% as significant and indicative of secondary structure changes since the error associated with the neglect of the Asn/Gln side chains is systematic and constant.

After 10 min, 80% of the amide groups were deuterated, and this percentage did not increase within 5 h. The residual amide bonds that remained hydrogenated are obviously buried in the interior of the protein and, hence, less accessible to the solvent.

Figure 2 shows the S- and A-maps derived from the 2D analysis of the FTIR spectra recorded as a function of time between 10 min and 5 h after dissolution of Cyt-*c*<sub>552</sub> in deuterated buffer. The white area represents spectral regions with no significant correlation. The peaks on the diagonal of the S-map reveal the bands that varied in absorbance as a function of time.

No correlation was observed in the amide-II range (1530–1545 cm<sup>-1</sup>), which is consistent with the results obtained by the deconvolution method that do not reveal any changes in the amide bond deuteration between 10 min and 5 h. Thus, the solvation processes of the protein under consideration are fast on the time scale of the time-dependent measurements (i.e., 5 h). Consequently, the variations revealed by the 2D correlation analysis are exclusively related to modes of amino acid side chain interacting with the solvent. As indicated by the magnitude of the autopeak, the main variation of absorbance is observed at 1605 cm<sup>-1</sup>, which corresponds to a Tyr ring mode. Most of the cross peaks observed in both S- and A-maps (Table 3) refer to this band as well as to those of Trp/His (1595 cm<sup>-1</sup>), Glu, and Asp (1575 and 1565 cm<sup>-1</sup>), implying that for some of these amino acids, solvation-induced rearrangements occur on the time scale of the FTIR experiments. The 1605/1595, 1605/1575, and 1605/1565-cm<sup>-1</sup> cross correlation peaks exhibit a positive sign in both the S- and A-maps indicating that the changes associated with Tyr follow those of Trp/His and Asp and Glu (see above). Only the cross peaks at 1625/1605, 1625/1595, and 1625/1575 cm<sup>-1</sup> indicate a variation of amide groups located in  $\beta$ -strand domains rather than variations of the Gln amide side chains, for which the corresponding mode is expected at higher wavenumbers

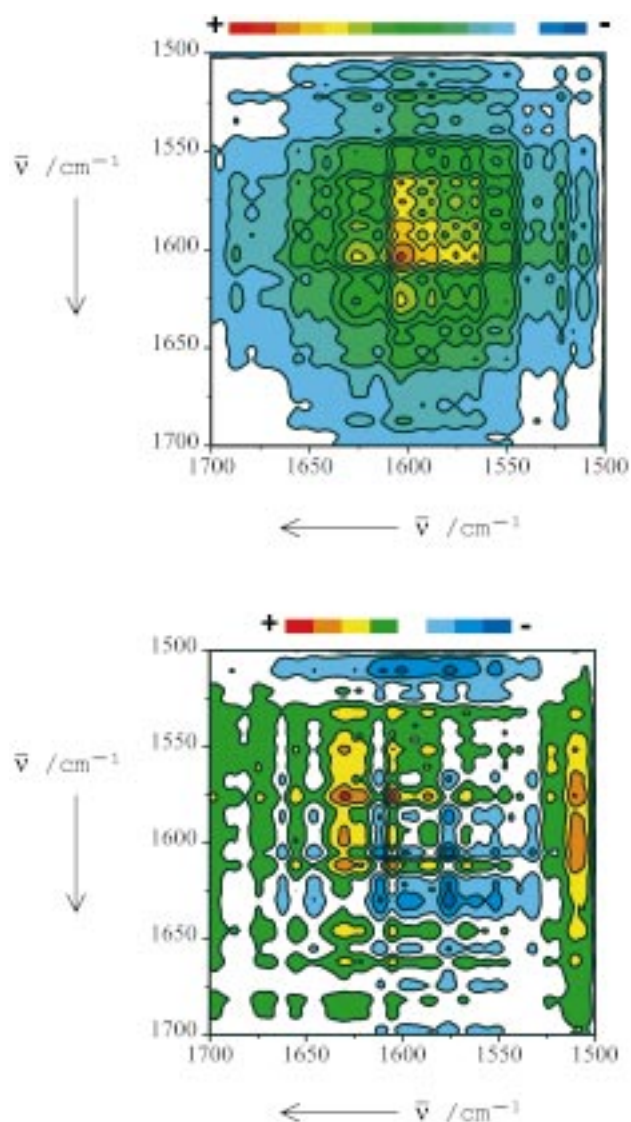


**Figure 2.** Synchronous and asynchronous representations of the FTIR spectra of Cyt- $c_{552}$  in deuterated buffer (pD 8.0). In the S-map (top), positive cross peaks are colored from turquoise to green to yellow to red, and negative cross peaks are colored in dark blue. In the A-map (bottom), positive cross peaks are colored from green to yellow to red, and negative cross peaks are colored from turquoise to dark blue. The white area in each map represents spectral regions with no significant correlation.

**Table 3.** Correlation between band wavenumbers (in  $\text{cm}^{-1}$ ) of Cyt- $c_{552}$  in solution at low ionic strength determined by 2D-FTIR spectroscopy.

Correlated bands and assignments <sup>[a]</sup>		sign (S) <sup>[b]</sup>	sign (A) <sup>[b]</sup>
$\nu_1$ (abscissa)	$\nu_2$ (ordinate)		
1625 ( $\beta$ -strands)	1605 (Tyr)	+	+
1625 ( $\beta$ -strands)	1595 (Trp, His)	+	+
1625 ( $\beta$ -strands)	1575 (Asp, Glu)	+	+
1605 (Tyr)	1595 (Trp, His)	+	+
1605 (Tyr)	1575 (Asp, Glu)	+	+
1605 (Tyr)	1565 (Asp)	+	+
1575 (Asp, Glu)	1565 (Asp)	+	-

[a] Only cross peaks observed in S- and A-maps were considered. [b] The signs of the cross correlation peaks in the S- and A-maps are denoted by "sign (S)" and "sign (A)", respectively.

( $1635\text{ cm}^{-1}$ ). The underlying intensity changes of these bands have the same direction as concluded from the positive signs of the cross peaks in the S-map. The same signs are observed in the A-map, implying that the perturbation in the  $\beta$ -strand domain occurs after the perturbation of the amino acid side chains.

Hence, it is concluded that the first events in the dynamics of the solvated protein (on the time scale accessible by the FTIR experiments) are perturbations of the Trp/His and Glu and Asp side chains followed by solvation changes of Tyr residues, which in turn affect the  $\beta$ -strand domains.

The crystal structure of Cyt- $c_{552}$ <sup>[7]</sup> provides deeper insight into the underlying solvation and structural changes. Figure 3 (bottom) shows a view of the back side of the protein surface (i.e., remote from the partly exposed heme edge). This region is predominantly formed by charged amino acids including Glu and Asp residues, which are possible candidates for the solvation-induced conformational changes reflected by the 2D analysis of the FTIR spectra. Among the four tyrosines of Cyt- $c_{552}$ ,

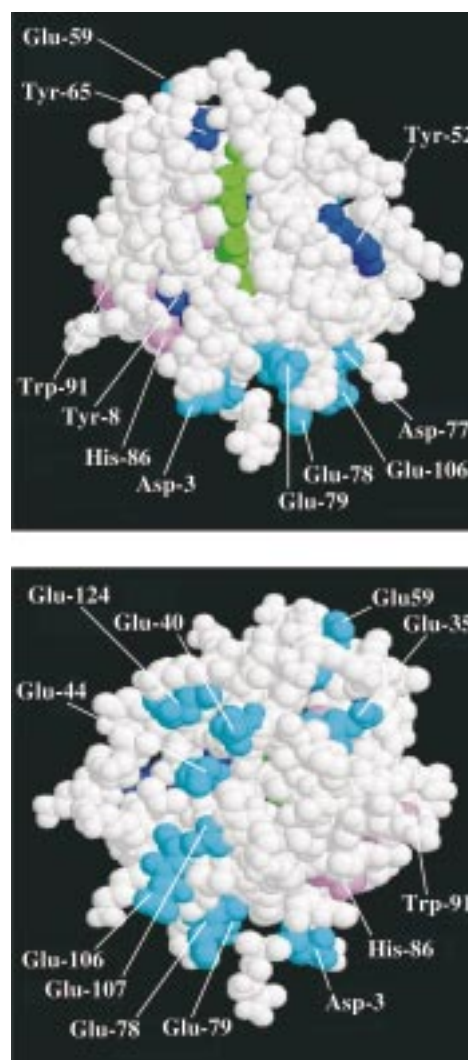


**Figure 3.** Space-filling plot of the structure of Cyt- $c_{552}$ <sup>[7]</sup> Tyr residues are shown in dark blue, Asp and Glu in cyan, and Trp and His in violet. Top: View of the front side including the heme site (green); bottom: view of the back side. The figures were prepared with program RASMOL.<sup>[33]</sup>



Tyr-45 is surrounded by hydrophobic side chains whereas Tyr-8, Tyr-52, and Tyr-65 are located in potentially more solvent-accessible regions of the protein.<sup>[7]</sup> While Tyr-8 is part of an  $\alpha$ -helix, Tyr-65 is part of the unique  $\beta$ -sheet domain (residues 54 to 69) (Figure 3, top), and Tyr-52 just forms the linkage between this  $\beta$ -sheet and the adjacent  $\alpha$ -helix. Thus, it is tempting to attribute the time-dependent changes of the 1605- $\text{cm}^{-1}$  band to Tyr-52 or Tyr-65 since these changes just precede those of the  $\beta$ -sheet amide-I band. In case of the assignment to Tyr-52, a solvation-induced conformational change of the aromatic side chain may trigger a slight extension of this  $\beta$ -sheet domain, whereas in the case of Tyr-65, the side chain conformational change may perturb the  $\beta$ -sheet structure in the immediate vicinity. Both effects could account for the 1625/1605- $\text{cm}^{-1}$  cross correlation peaks.

For the assignment of the 1595- $\text{cm}^{-1}$  band to a specific Trp or His residue, the most likely candidates are Trp-91 and His-86 or His-32 since all of them are accessible to the solvent.<sup>[7]</sup> None of these residues is located close to the  $\beta$ -sheet segment 54–69 so that the assignment to either Trp-91 or His residues is equally plausible.

At high ionic strength (0.5  $\text{mol L}^{-1}$  KCl), a deuteration degree of 80% is reached after 10 min, but it further increases to 84% after 5 h which is slightly higher than at low ionic strength (80%). This time-dependent change is also revealed by the 2D-FTIR analysis as the S-map displays a dominant cross peak in the range of 1530–1555  $\text{cm}^{-1}$  (Figure 4) which is attributed to a slow H/D exchange of amide NH groups in buried regions of the protein. Such an additional slow H/D exchange was not observed for Cyt- $c_{552}$  dissolved at low ionic strength since the degree of deuteration was found to be the same after 10 min and 5 h, and no cross peak in the amide-II region was observed.

The only notable cross correlation peak attributable to an amino acid side chain band refers to the intensity changes of the Tyr band at 1605  $\text{cm}^{-1}$ . These changes follow the slow phase of the amide H/D exchange as indicated by the correlation peak observed at 1605/1545  $\text{cm}^{-1}$ . Thus, these changes may be associated with a Tyr residue located in the interior of the protein, for which Tyr-45 is the only candidate.

At high ionic strength more buried peptide segments become accessible to H/D exchange, albeit at a smaller rate, which may indicate a slight loosening of the tertiary structure. However, the secondary structure of the protein as well as the solvation-induced conformational changes are the same at low and high ionic strength (Table 2).

#### Adsorption on talc

Table 4 lists the percentage of peptide bonds involved in different secondary structure elements for Cyt- $c_{552}$  adsorbed on TC. The results do not differ for TC–Cyt- $c_{552}$  suspensions in buffer and for solid TC–Cyt- $c_{552}$  samples obtained after centrifugation. As no protein was detected in the supernatant, it is concluded that all the protein is adsorbed on TC at the Cyt- $c_{552}$ /TC mass ratio of 4:200 used in these experiments. Taking into account the specific area of TC of 18.5  $\text{m}^2 \text{g}^{-1}$ , one obtains a coverage of one Cyt- $c_{552}$  molecule per 2000  $\text{\AA}^2$ . This value is substantially larger

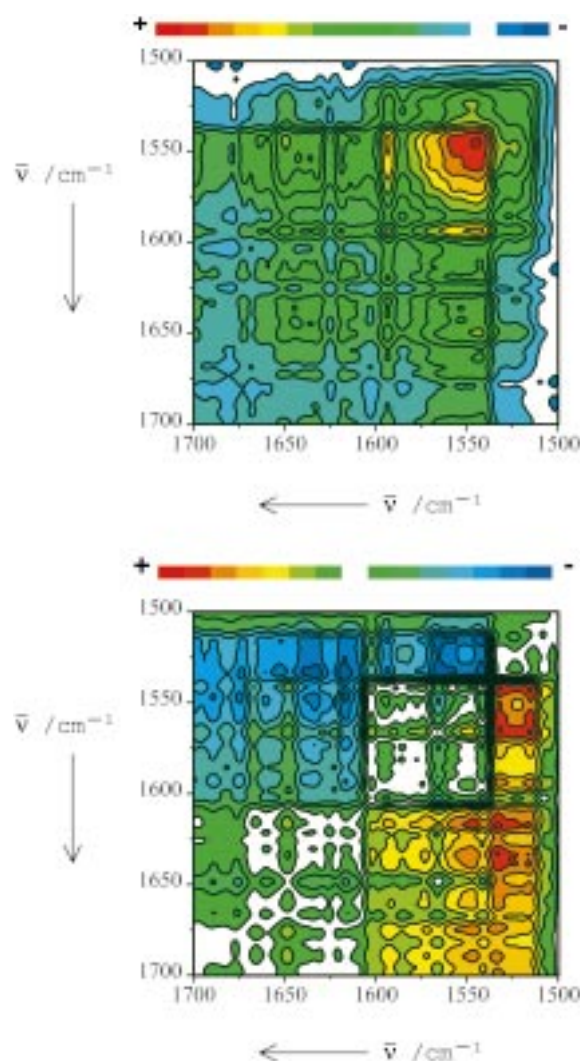


**Figure 4.** Synchronous (top) and asynchronous (bottom) representations of the FTIR spectra of Cyt- $c_{552}$  in deuterated buffer (pD 8.0) with 0.5  $\text{mol L}^{-1}$  KCl. The color code is the same as that in Figure 2.

than the minimum area of ca. 800  $\text{\AA}^2$  required by one bound protein molecule as judged from the crystal structure.<sup>[7]</sup> Therefore, adsorption of Cyt- $c_{552}$  to TC is possible without protein–protein interactions. In fact, the analysis of the FTIR spectra of Cyt- $c_{552}$ /TC measured under equilibrium conditions (i.e., after 5 h; see above) reveals only a small intensity increase (ca. 3%) of the 1612- $\text{cm}^{-1}$  band that is indicative of amide groups involved in protein self-association.

On the other hand, there are distinct changes of the secondary structure for Cyt- $c_{552}$  adsorbed on TC compared to the protein in solution (see Table 4). The band component at 1630  $\text{cm}^{-1}$  increases from ca. 21 to 27% at the expense of the band components at 1660 and 1638  $\text{cm}^{-1}$  that decrease from 26 to 21% and from 11 to 6%, respectively. We assigned these variations to an increase in the number of peptide groups involved in  $\beta$ -strand/turn structure and a decrease in the number of peptide groups involved either in  $\alpha$ -helical structure or located in hydrated random-coil domains. Conversely, potential contributions of Gln and Asn side chain bands to these spectral

**Table 4.** Secondary structure elements for Cyt-*c*<sub>552</sub> in solution or adsorbed on TC or MT.

Secondary structure element	Relative contribution [%] <sup>[a]</sup>						
	solution <sup>[b]</sup>	suspension <sup>[c]</sup>		solid <sup>[d]</sup>		solid (+ KCl) <sup>[e]</sup>	
			TC	MT	TC	MT	TC
β-strands in apolar domains not hydrogen-bonded inside the protein core	1.5	1.0	2.3	2.2	2.0	0.9	1.2
hydrogen-bonded in irregular/internal α-helix	9.0	8.3	7.6	8.7	9.0	8.0	7.6
hydrogen-bonded in external/regular α-helix	26.5	21.8	23.9	20.6	23.8	21.3	25.3
hydrated in random-coil domains	22.9	24	22.4	23.0	22.0	24.3	23.1
hydrogen-bonded in β-strands or turns	10.8	6.8	10.8	5.4	10.5	6.5	12.8
hydrogen-bonded in protein self-association	20.8	26.9	22.9	28.4	23.2	29.1	21.6
	8.5	11.2	10.1	11.7	9.5	9.9	8.4

[a] The accuracy of the secondary structure determination is discussed in the text. [b] Sample 1 (see Table 2) as reference for comparison with adsorbed species. [c] Cyt-*c*<sub>552</sub>-TC or Cyt-*c*<sub>552</sub>-MT suspension in deuterated buffer (after 5 h). [d] Sample obtained after centrifugation of the suspension. [e] Sample obtained after centrifugation of a suspension containing 0.5 mol L<sup>-1</sup> KCl.

changes are likely to be small since interactions of these residues with hydrophobic surfaces would cause wavenumber upshifts of their amide bands into the region where we observe an intensity reduction.<sup>[20]</sup> Thus, altogether, these changes refer to ca. 10% of the backbone corresponding to ca. 12–13 peptide units.

Furthermore, adsorption on TC favors the NH/ND exchange since the extent of deuteration after 5 h is higher by 4% than for the dissolved protein. Addition of KCl (0.5 mol L<sup>-1</sup>) induces only a partial desorption of the protein (30%) from the surface, implying that binding of Cyt-*c*<sub>552</sub> to the uncharged TC surface is largely governed by hydrophobic interactions. The crystal structure of Cyt-*c*<sub>552</sub> reveals two hydrophobic regions on the front surface close to the heme which are both possible candidates for the interaction domain with TC.<sup>[7]</sup> One domain involves the hydrophobic β-strands (Gly-19–Pro-27) close to the larger reversed β-strands (Met-63–Leu-75) and the second one is constituted by the N-terminal helix (Ala-2–Ala-9). This latter peptide segment involves several Ala and Ile residues which can easily be orientated towards the hydrophobic TC surface. Furthermore, in close proximity to the reversed Met-63–Leu-75 β-strand, the N-terminal segment includes an α-helical portion which upon transition to β-sheet structure would contribute to the energetically favorable formation of a more extended β-sheet domain. These secondary structure changes could account for the increase of β-sheet at the expense of α-helical structure as observed upon binding to TC.

The time-dependent 2D-FTIR analysis reveals no correlation peaks for marker bands of the α-helical structures (Figure 5) implying that the decrease of the α-helical content upon adsorption to TC occurs within less than 10 min. The cross peaks observed on both the S-map and A-map are listed in Table 5. The first events that can be derived from the 2D-FTIR maps involve the Tyr band at 1605 cm<sup>-1</sup> and the Asp/Glu bands at 1585, 1575, and 1565 cm<sup>-1</sup> that are subject to spectral changes prior to those of the β-strand amide-I band. The order of these events is reminiscent of those found for Cyt-*c*<sub>552</sub> in solution suggesting that also the underlying molecular changes are similar to the dissolved Cyt-*c*<sub>552</sub>. In fact, the charged amino acid clusters are not in the vicinity of the putative domains of α-helix unfolding and β-sheet folding. Thus, the response of these residues to solvation is not expected to be different to that of the dissolved Cyt-*c*<sub>552</sub>. This may also be true for Tyr-52 and Tyr-65 which are

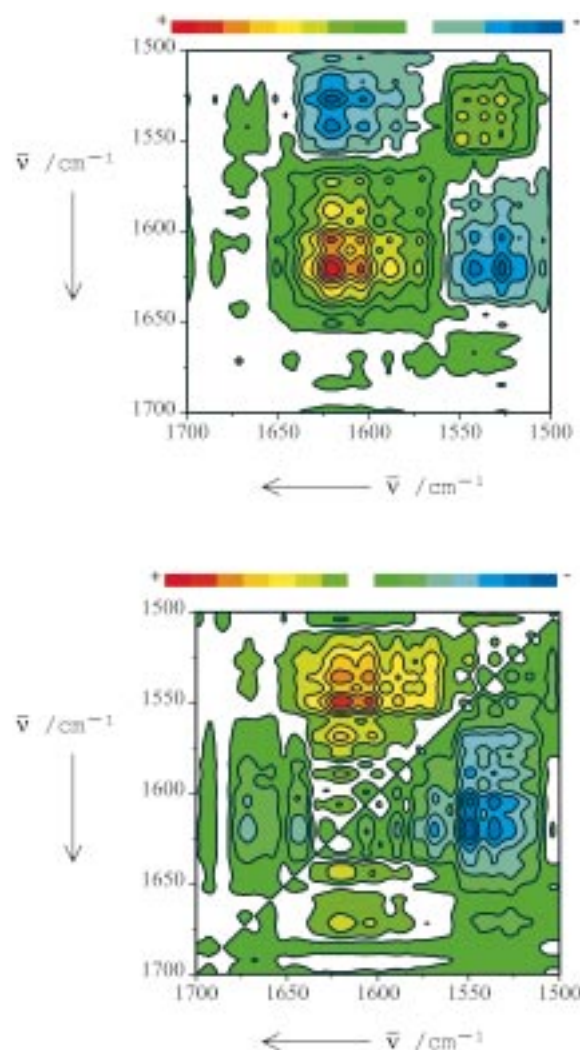


**Figure 5.** Synchronous and asynchronous representations of the FTIR spectra of Cyt-*c*<sub>552</sub>-TC in deuterated buffer (pD 8.0). The color code is the same as that in Figure 2.

located at the periphery of the hydrophobic domains so that, by analogy with the dissolved protein, the 1605-cm<sup>-1</sup> peak in the 2D-FTIR maps may be ascribed to one of these residues. The correlations between the amide-II bands (1530 and 1545 cm<sup>-1</sup>)

**Table 5.** Correlation between band wavenumbers (in  $\text{cm}^{-1}$ ) of Cyt- $c_{552}$  adsorbed on TC determined by 2D-FTIR spectroscopy.

Correlated bands and assignments <sup>[a]</sup>			
$\nu_1$ (abscissa)	$\nu_2$ (ordinate)	sign (S) <sup>[b]</sup>	sign (A) <sup>[b]</sup>
1625 ( $\beta$ -strands)	1605 (Tyr)	+	+
1625 ( $\beta$ -strands)	1590 (Glu)	+	+
1625 ( $\beta$ -strands)	1575 (Glu, Asp)	+	+
1625 ( $\beta$ -strands)	1545 (amide II)	-	+
1625 ( $\beta$ -strands)	1530 (amide II)	-	+
1605 (Tyr)	1590 (Glu)	+	+
1605 (Tyr)	1575 (Glu, Asp)	+	+
1605 (Tyr)	1545 (amide II)	-	+
1605 (Tyr)	1530 (amide II)	-	+
1550 (amide II)	1530 (amide II)	+	+

[a] Only cross peaks observed in S- and A-maps were considered. [b] The sign of the cross correlation peaks in the S- and A-maps are denoted by "sign (S)" and "sign (A)", respectively.

and the Tyr ( $1605\text{ cm}^{-1}$ ) and the  $\beta$ -strand amide-I bands ( $1625\text{ cm}^{-1}$ ) and the signs of the cross peaks imply that the enlargement of the  $\beta$ -sheet structure is followed by a further H/D exchange. These slowly exchanged protons are attributed to amide bonds in the binding domain which obviously become accessible only after a reorganization of the secondary structure. Consistent with this interpretation is the observation that the extent of deuteration after 10 min is the same as for Cyt- $c_{552}$  in solution (i.e., 80%). The exchange in the slow phase just accounts for the additional portion of deuterated amide bonds (4%).

Similar to Cyt- $c_{552}$  in solution, addition of  $0.5\text{ mol L}^{-1}$  KCl to the TC-Cyt- $c_{552}$  suspension leads to a further increase in the H/D exchange to ca. 90%. No structural differences are noted compared to the suspension at low ionic strength.

### Adsorption on montmorillonite

At a Cyt- $c_{552}$ /MT ratio of 1:2 (w/w) and at low ionic strength, essentially all the protein is adsorbed to the anionic clay since after centrifugation no protein was detected in the supernatant. Furthermore, no differences (within 1%) were obtained for the Cyt- $c_{552}$ -MT suspension and the centrifuged sample (Table 4). On the other hand, the amount of adsorbed protein is reduced to 30% after addition of  $0.5\text{ mol L}^{-1}$  KCl. These findings indicate that Cyt- $c_{552}$  binding to the negatively charged surface of MT is largely controlled by electrostatic forces. Hence, it is reasonable to assume that adsorption does not involve the same part of the protein surface as is the case with binding to TC. Instead, it is very likely that binding to MT occurs through cationic residues.

Most of the positively charged amino acids (Arg and Lys) are located in two domains on the back side of the protein, that is, opposite to the more hydrophobic domain.<sup>[7]</sup> One domain involves Lys-109, Lys-110, Lys-114, and Lys-115 and Arg-112 close to Lys-76, while Lys-95, Lys-96, Lys-98, and Lys-101 constitute the second domain. Lys-109 and Lys-110 are part of an  $\alpha$ -helix, whereas the other Lys residues are located in less structured or  $\beta$ -sheet domains.

The analysis of the FTIR spectra measured under equilibrium conditions reveals only small changes of secondary structure upon adsorption to MT (see Table 4). The only significant amide-I intensity change is the slight decrease of the  $1660\text{-cm}^{-1}$  component that is attributable to peptide bonds in an irregular  $\alpha$ -helix. It is tempting to assign this decrease to the small  $\alpha$ -helical segment involving Lys-109 and Lys-110 on the back side of the protein (see above), since adsorption is likely to affect specifically the structure in the interaction domain. Furthermore, adsorption on MT hinders the H/D exchange since after 5 h the extent of deuteration is smaller by 3% than for the dissolved protein. Note that also for mitochondrial Cyt- $c$  no significant secondary structure changes were observed upon binding to negatively charged surfaces (i.e., phospholipid vesicles), whereas in contrast to Cyt- $c_{552}$  the H/D exchange rate is substantially increased.<sup>[21, 22]</sup>

The 2D analysis (Figure 6, Table 6) reveals no correlation for amide-I bands of  $\alpha$ -helical structure elements implying that the structural perturbation in the binding domain occurs within

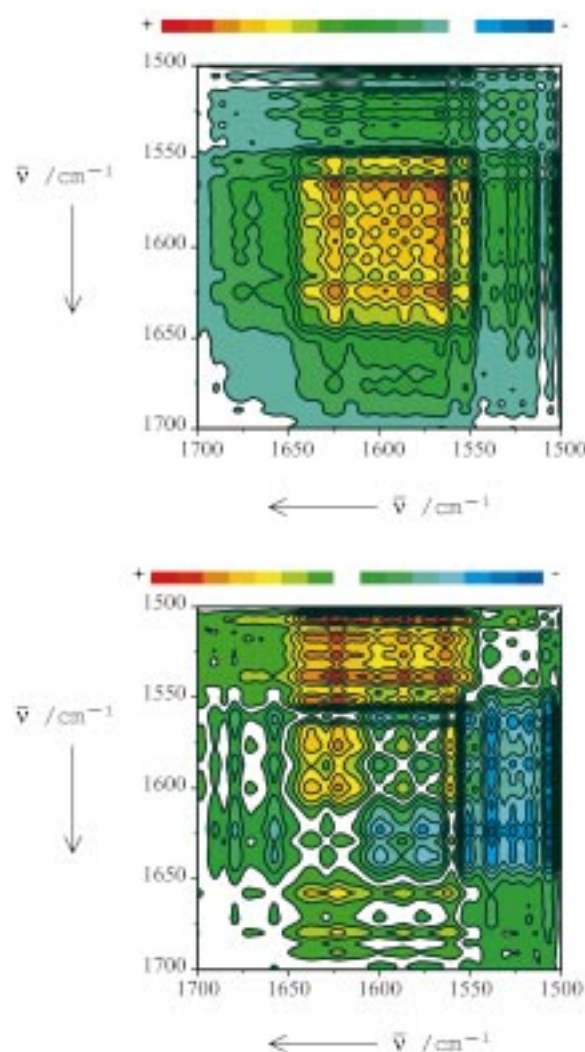


**Figure 6.** Synchronous and asynchronous representations of the FTIR spectra of Cyt- $c_{552}$ -MT in deuterated buffer (pD 8.0). The color code is the same as that in Figure 2.



**Table 6.** Correlation between band wavenumbers (in  $\text{cm}^{-1}$ ) of Cyt- $c_{552}$  adsorbed on MT determined by 2D-FTIR spectroscopy.

Correlated bands and assignments <sup>[a]</sup>			
$\nu_1$ (abscissa)	$\nu_2$ (ordinate)	sign (S) <sup>[b]</sup>	sign (A) <sup>[b]</sup>
1625 ( $\beta$ -strand)	1605 (Tyr)	+	+
1625 ( $\beta$ -strand)	1585 (Glu)	+	+
1625 ( $\beta$ -strand)	1565 (Asp)	+	+
1625 ( $\beta$ -strand)	1555 (amide II)	+	+
1605 (Tyr)	1585 (Glu)	+	-
1605 (Tyr)	1565 (Asp)	+	-
1605 (Tyr)	1555 (amide II)	+	+
1585 (Glu)	1565 (Asp)	+	-
1585 (Glu)	1555 (amide II)	+	+
1565 (Asp)	1555 (amide II)	+	+

[a] Only cross peaks observed in S- and A-maps were considered. [b] The sign of the cross correlation peaks in the S- and A-maps are denoted by "sign (S)" and "sign (A)", respectively.

10 min after adsorption. The changes that are detectable by 2D-FTIR spectroscopy are related to Tyr, Glu, and Asp side chains. They are correlated with changes of the amide-II band and the amide-I component at  $1625\text{ cm}^{-1}$  that refer to peptide bonds in  $\beta$ -structures. According to the signs in the S- and A-maps, the amide-II band change, which would correspond to a slow phase of H/D exchange on the time scale of five hours, precedes those of the amino acid side chains which in turn are followed by a change of the  $\beta$ -turn domain. Note that the band-fitting analysis of the FTIR spectra measured after 10 min and 5 h reveals a subtle increase in  $\beta$ -turn structure by ca. 1.5% (2 peptide bonds) which, however, is at the limit of experimental accuracy. This finding indicates that the 2D analysis may be capable of identifying subtle structural changes in a more reliable manner than conventional deconvolution and band-fitting methods.

To probe the effect of KCl on the structure of the adsorbed Cyt- $c_{552}$ , the suspension containing  $0.5\text{ mol L}^{-1}$  KCl was centrifuged to remove the desorbed protein. The FTIR spectra of the Cyt- $c_{552}$ -MT-KCl precipitate indicate that the  $\alpha$ -helical content and the degree of H/D exchange is essentially the same as for Cyt- $c_{552}$  dissolved at high ionic strength. It may be that the interactions between the positively charged regions of the protein and the negatively charged MT surface are mediated by cations and anions.

### Electrostatic and hydrophobic binding of cytochrome $c_{552}$

Cyt- $c_{552}$  can effectively bind to the respective anionic and apolar surfaces of MT and TC through two different binding domains. Electrostatic binding of Cyt- $c_{552}$  to negatively charged surfaces involves a lysine cluster on the back side of the protein, that is, remote from the heme pocket. These interactions produce only subtle changes in the secondary structure (ca. 3%). Mitochondrial Cyt- $c$  also binds to negatively charged surfaces such as phospholipid vesicles through a lysine-rich region of the protein surface without detectable perturbation of the secondary structure.<sup>[21, 22]</sup> However, for Cyt- $c$  such electrostatic interactions not only with phospholipid headgroups but also with polyanions and negatively charged electrodes have been shown to

induce substantial structural changes in the heme pocket that is close to the interaction domain.<sup>[23-26]</sup> Specifically, a new conformational state (state B2), lacking the axial Met ligand, is formed that is in equilibrium with the native form of the protein (state B1).<sup>[3, 4, 23-26]</sup> For Cyt- $c_{552}$ , comparable perturbations of the heme site, albeit to a much smaller extent, have only been found upon adsorption to electrodes.<sup>[9]</sup> Binding to MT leaves the heme pocket structure of Cyt- $c_{552}$  unchanged as revealed by a resonance Raman spectroscopic analysis (spectra not shown here). The different response of the heme site of Cyt- $c_{552}$  to electrostatic interactions, as compared to Cyt- $c$ , may be due to the higher intrinsic protein stability and to the larger distance of the heme from the charged interface.

The interaction domain for TC is ascribed to a hydrophobic region on the front surface of Cyt- $c_{552}$ . In the Cyt- $c_{552}$ -TC complexes, more pronounced secondary structural changes are observed as compared to Cyt- $c_{552}$  electrostatically bound on MT. Specifically, the  $\beta$ -sheet structure is increased at the expense of the  $\alpha$ -helical content. Hydrophobic binding to TC, which is evidently entropy-driven, must be associated with a relatively large binding constant since at the Cyt- $c_{552}$ /TC concentration ratio used in the FTIR experiments, a large surface coverage is achieved with negligible amounts of protein left in solution.

Hydrophobic interactions that include secondary structure changes have also been suggested to play role for Cyt- $c$  upon binding to phospholipids at high ionic strength,<sup>[27]</sup> although for that protein a specific hydrophobic domain has not yet been identified.

### Implications for the reaction of cytochrome $c_{552}$ with $ba_3$ -oxidase

For mitochondrial Cyt- $c$  the lysine-rich region around the exposed heme edge has been identified as the binding domain for CcO and cytochrome  $c$  reductase.<sup>[1, 2]</sup> Hence, complex formation with these enzymes requires an anionic binding domain on the partner proteins. This region has been recently identified for CcO from *Paracoccus denitrificans* and, indeed, has been shown to include several negatively charged amino acids (Asp-135, Asp-159, Asp-178, Asp-257, and Glu-126).<sup>[28]</sup> Furthermore, complex formation through these oppositely charged binding domains provides the shortest possible distance for interprotein electron transfer from the heme group of Cyt- $c$  to the  $\text{Cu}_A$  center of CcO.<sup>[28, 29]</sup>

In the case of Cyt- $c_{552}$ , such an arrangement is not possible for the complex with the  $ba_3$ -oxidase since the lysine-rich domain responsible for electrostatic binding is located remote from the heme site. Moreover, the crystal structure of  $ba_3$ -oxidase does not reveal a binding domain that exhibits the required charge complementarity.<sup>[8]</sup> In contrast to other cytochrome  $c$  oxidases, Asp-135 and Asp-159 are not conserved in  $ba_3$ -oxidase and there are no other negatively charged amino acid residues that might constitute a possible anionic domain. Instead, the region on the protein surface close to the electron acceptor predominantly involves amino acids of apolar and hydrophobic character and, in this respect, this region mirrors the hydrophobic binding domain of Cyt- $c_{552}$ . As this latter region is located close to the

heme pocket, a complex with  $ba_3$ -oxidase that is formed through these hydrophobic domains would lead to a distance between electron acceptor and donor sites that is approximately as short as in the electrostatically stabilized complexes between Cyt- $c$  and CcO. These considerations suggest that complex formation between Cyt- $c_{552}$  and  $ba_3$ -oxidase occurs through hydrophobic rather than electrostatic interactions. This conclusion is in line with kinetic studies of the Cyt- $c_{552}$ - $ba_3$ -oxidase reaction that have shown an increasing enzymatic activity with decreasing ionic strength.<sup>[6]</sup> For an electrostatically stabilized complex such as CcO-Cyt- $c$ , the decrease of the ionic strength slows down the dissociation rate for the complex and, hence, reduces the enzymatic activity.<sup>[1]</sup>

Since hydrophobic interactions control binding of Cyt- $c_{552}$  to the  $ba_3$ -oxidase, the hydrophobic surface of TC may be regarded as a model for the docking domain of the  $ba_3$ -oxidase. Adsorption of Cyt- $c_{552}$  on TC leads to a change of the secondary structure attributed to 6 to 7 amide bonds, obviously in the binding domain, that are transformed from an  $\alpha$ -helical to a  $\beta$ -sheet structure. Whereas unfolding of the helical segment (possibly, Ala-2 – Ala-9) is too fast to be detectable in the present FTIR experiment, the subsequent formation of the extended  $\beta$ -sheet domain in any protein molecule proceeds on a time scale of hours. Thus, such a refolding process is certainly too slow to be of relevance for the interaction of Cyt- $c_{552}$  with  $ba_3$ -oxidase under physiological conditions. Whether or not this is also true for the unfolding of the  $\alpha$ -helical segment cannot be assessed based on the present experiments due to a time resolution limit of 10 min. On the other hand, it is known that unfolding of a relatively small peptide segment may occur within tenths of microseconds.<sup>[30]</sup> Therefore, the structural reorganization of the small  $\alpha$ -helical segment in the hydrophobic binding domain might take place on the same time scale as the electron transfer from Cyt- $c_{552}$  to  $ba_3$ -oxidase, for which a rate constant of  $10^4$  –  $10^5$  s<sup>-1</sup> is estimated based on the comparison with kinetic data for the mitochondrial Cyt- $c$ /CcO redox couple.<sup>[5, 9, 31, 32]</sup> Following these considerations it may be that structural reorganization of Cyt- $c_{552}$ , as observed in the complex with TC, is of functional relevance for interprotein electron transfer to the oxidase, for instance, by allowing a proper alignment of the redox partners. This interpretation may account for the high specificity of the reaction of Cyt- $c_{552}$  with  $ba_3$ -oxidase, which cannot be reduced by mitochondrial Cyt- $c$ .<sup>[5]</sup>

*P.H. acknowledges a Heisenberg stipend from the Deutsche Forschungsgemeinschaft.*

- [1] G. W. Pettigrew, G. R. Moore, *Cytochrome c—Biological Aspects*, Springer, Berlin, 1987.
- [2] R. A. Scott, A. G. Mauk, *Cytochrome c—A Multidisciplinary Approach*, University Science Books, Sausalito, CA, USA, 1995.
- [3] S. Döpner, P. Hildebrandt, F. I. Rosell, A. G. Mauk, M. von Walter, G. Buse, T. Soulimane, *Eur. J. Biochem.* **1999**, *261*, 379–391.
- [4] H. Wackerbarth, U. Klar, W. Günther, P. Hildebrandt, *Appl. Spectrosc.* **1999**, *53*, 283–291.
- [5] T. Soulimane, M. von Walter, P. Hof, M. E. Than, R. Huber, G. Buse, *Biochem. Biophys. Res. Commun.* **1997**, *237*, 572–576.
- [6] A. Giuffrè, E. Forte, G. Antonini, E. D'Itri, M. Brunori, T. Soulimane, G. Buse, *Biochemistry* **1999**, *38*, 1057–1065.
- [7] M. E. Than, P. Hof, R. Huber, G. P. Bourenkov, H. D. Bartunik, G. Buse, T. Soulimane, *J. Mol. Biol.* **1997**, *271*, 629–644.
- [8] T. Soulimane, G. Buse, G. P. Bourenkov, H. D. Bartunik, R. Huber, M. E. Than, *EMBO J.* **2000**, *19*, 1766–1776.
- [9] S. Lecomte, P. Hildebrandt, T. Soulimane, *J. Phys. Chem. B* **1999**, *103*, 10053–10064.
- [10] L. Boulkanz, L. Balcar, M. H. Baron, *Appl. Spectrosc.* **1995**, *49*, 1737–1746.
- [11] I. Noda, *Appl. Spectrosc.* **1990**, *44*, 550–561.
- [12] P. Chassin, C. Jouany, H. Quiquampoix, *Clay Miner.* **1986**, *21*, 899–907
- [13] W. B. Kleijn, J. D. Oster, *Clays Clay Miner.* **1982**, *30*, 383–389.
- [14] D. Baron, *Logiciels pour la chimie*, Societe Française de Chimie, Paris, **1991**, p. 282.
- [15] M. H. Baron, M. Revault, S. Servagent-Noinville, J. Abadie, H. Quiquanpoix, *J. Colloid Interface Sci.* **1999**, *214*, 319–333.
- [16] W. K. Surewicz, H. H. Mantsch, *Biochim. Biophys. Acta* **1988**, *952*, 115–130.
- [17] a) S. Y. Venyaminov, N. N. Kalnin, *Biopolymers* **1990**, *30*, 1243–1257; b) Y. N. Chirgadze, O. V. Fedorov, N. P. Trushina, *Biopolymers* **1975**, *14*, 679–694; c) S. A. Sukhishvili, S. Granick, *J. Chem. Phys.* **1999**, *110*, 10153–10161.
- [18] J. Wantyghem, M. H. Baron, M. Picquart, F. Lavielle, *Biochemistry* **1990**, *29*, 6608–6609.
- [19] M. H. Baron, C. de Loze, C. Toniolo, G. D. Fasman, *Biopolymers* **1978**, *17*, 2225–2239.
- [20] F. Fillaux, C. de Loze, *Biopolymers* **1972**, *11*, 2063–2077.
- [21] A. Muga, H. H. Mantsch, W. K. Surewicz, *Biochemistry* **1991**, *30*, 7219–7224.
- [22] T. Heimburg, D. Marsh, *Biophys. J.* **1993**, *65*, 2408–2417.
- [23] G. Chottard, M. Michelon, M. Hervé, G. Hervé, *Biochim. Biophys. Acta* **1987**, *916*, 402–410.
- [24] P. Hildebrandt, M. Stockburger, *Biochemistry* **1989**, *28*, 6710–6721.
- [25] P. Hildebrandt, T. Heimburg, D. Marsh, *Eur. Biophys. J.* **1990**, *18*, 193–201.
- [26] P. Hildebrandt, *Biochim. Biophys. Acta.* **1990**, *1040*, 175–186.
- [27] J. D. Cortese, A. L. Voglino, C. R. Hackenbrock, *Biochemistry* **1998**, *37*, 6402–6409.
- [28] H. Witt, F. Malatesta, F. Nicoletti, M. Brunori, B. Ludwig, *Eur. J. Biochem.* **1998**, *251*, 367–373.
- [29] S. Iwata, C. Ostermeier, B. Ludwig, H. Michel, *Nature* **1995**, *376*, 660–669.
- [30] M. C. R. Shastry, J. M. Sauder, H. Roder, *Acc. Chem. Res.* **1998**, *31*, 717–725.
- [31] T. Soulimane, G. Buse, *Eur. J. Biochem.* **1995**, *227*, 588–595.
- [32] L. M. Geren, J. R. Beasley, B. R. Fine, A. J. Saunders, S. Hibdon, G. J. Pielak, B. Durham, F. Millett, *J. Biol. Chem.* **1995**, *270*, 2466–2474.
- [33] R. A. Sayle, E. J. Milner-White, *Trends Biochem. Sci.* **1995**, *20*, 374.

Received: April 25, 2000

Revised version: October 18, 2000 [F 48]